NWRI-UNPUBLISHED MANUSCRIPT
LAU, YL 1980

LAU

Environment Canada

Environnement Canada

National Water Research Institute

Institut National de Recherche sur les Eaux

EFFECT OF ICE COVER ON STREAM FLOWS AND VERTICAL MIXING

by

Y. L. Lau and B. G. Krishnappan

TD
7
L38
1980a

This manuscript has been submitted to the
Journal of the Hydraulics Division, ASCE
for publication and the contents
are subject to change.

This copy is to provide information
prior to publication.

EFFECT OF ICE COVER ON STREAM FLOWS AND VERTICAL MIXING

by

Y. L. Lau and B. G. Krishnappan

Environmental Hydraulics Section
Hydraulics Research Division
National Water Research Institute
Canada Centre for Inland Waters
April 1980

MANAGEMENT PERSPECTIVE

When a river changes from free-surface flow to ice-covered flow, most of the flow characteristics are changed, including the flow depth, velocity and shear stress distributions as well as the diffusivity distribution. While some of the existing analytical models of ice-covered flows can give reasonable descriptions of the velocity and shear stress distributions, the resulting profiles of mass and momentum diffusivities are entirely erroneous and cannot be applied to mixing problems for ice-covered flows.

In this report a turbulence model is used to calculate the flow structure for both free-surface and ice-covered conditions. It is shown that, in order to carry the same discharge, the flow depth will increase by about 10% to 30% when ice cover is present. The model also provides realistic predictions of the eddy diffusivity profiles. The results indicate that the mixing capacity of a stream is reduced when it becomes ice-covered and that this reduction in mixing is most pronounced if material is released into the flow at the top.

This model can be used to predict the changes which occur when a river becomes ice-covered and can be an aid in planning and management.

Y. L. Lau, Head
Environmental Hydraulics Section
Hydraulics Division
September 1980

PERSPECTIVE - GESTION

Lorsque l'écoulement d'une rivière passe d'un écoulement à surface libre à un écoulement recouvert de glace, la plupart des caractéristiques de l'écoulement sont modifiées, y compris la profondeur de l'écoulement, la vélocité et les répartitions de l'effort de cisaillement de même que la distribution de la diffusivité. Bien que certains des modèles analytiques actuels des écoulement recouverts de glace puissent offrir d'assez bonnes descriptions de la vélocité et des répartitions de l'effort de cisaillement, les profils de diffusivité de la masse et de la quantité de mouvement qui en découlent sont entièrement erronés et ne peuvent être appliqués aux problèmes de mélange pour les écoulements recouverts de glace.

Dans le présent rapport, un modèle de turbulence est utilisé pour calculer la structure de l'écoulement à la fois dans des conditions d'écoulement à libre surface et d'écoulement recouvert de glace. On montre que pour transporter le même débit, la profondeur de l'écoulement augmentera d'environ 10 p. 100 à 30 p. 100, lorsque la couverture de glace est présente. Le modèle fournit aussi des prévisions réalistes sur les profils de diffusion tourbillonnaire. Les résultats indiquent que la capacité de mélange d'un cours d'eau est réduite lorsqu'il est recouvert de glace et que cette réduction du mélange est plus pronouncée lorsque des matériaux sont déversés dans l'écoulement au sommet.

Ce modèle peut être utilisé pour prévoir les changements survenant lorsqu'une rivière est recouverte de glace et peut être utile pour la planification et la gestion.

Y. L. Lau, Chef
Section de l'hydraulique environnementale
Division de l'hydraulique
Septembre 1980

KEYWORDS: channels (waterways), computation, dispersion equivalent, free-surface flow, ice-covered flow, jet-type discharge, numerical scheme, turbulence model.

ABSTRACT: The distributions of velocity, turbulent eddy and mass diffusivities were computed for three pairs of free-surface and ice-covered flows using the k-ε turbulence model. The flow rate, the channel slope and the bottom roughness values were kept the same for each pair and the flow depths were computed. The resulting flow depths for ice-covered flows were 15 to 30 percent higher than the depths for the free-surface flows.

The computed velocity and diffusivity distributions do not follow the conventional logarithmic and parabolic distributions for the whole depth of flow. The velocity distribution deviates slightly from the logarithmic profile for the top 25 percent of the flow while the diffusivity distribution deviates from parabolic distribution through the top half of the flow. These results are in general agreement with recent investigations on velocity distributions and the measurement of diffusivity distributions.

Concentration distributions resulting from the introduction of a neutrally buoyant tracer were computed for all the flows and these distributions indicate reduced mixing rates in ice-covered flows compared to free-surface flows. However, the results from using a jet-type injection gave approximately the same concentrations for both cases indicating the effects of jet mixing outweigh the difference in the diffusivity.

MOTS CLÉS: Chenaux (voies navigables), calcul, dispersion équivalente, écoulement à surface libre, écoulement recovert de glace, débit du type het, plan numérique, modèle de turbulence.

SOMMAIRE: Les distributions de la vélocité, du tourbillon de turbulence et des diffusivités de masse ont été comparées dans le cas de trois paires d'écoulement à surface libre ou recouvert de glace en utilisant le modèle de turbulence K- . On a gardé pour chaque paire les valeurs du débit de l'écoulement, de la pente du chenal et de l'irrégularité du fond et on a calculé les profondeurs de l'écoulement. Les profondeurs des écoulements recouverts de glace étaient de 15 à 30 p. 100 supérieures à celles des écoulements à surface libre.

La vélocité ainsi que les distributions de diffusivité calculées ne respectent pas les réparitions logarithmiques et paraboliques conventionnelles pour la profondeur globale de l'écoulement. La répartition de la vélocié est légèrement differente du profil logarithmique pour les 25 p. 100 supérieurs de lécoulement, alors que la répartition de la diffusivité s'écarte de la répartition parabolique dans la moitié supérieure de l'écoulement. Ces résultats concordent en général avec les récentes études sur la répartition de la vélocité et la mesure des répartitions de diffusivité.

Les répartitions de concentration provenant de l'introduction d'un traceur neutre sur le plan de la flottaison ont été calculées pour tous les écoulements et ces répartitions révélent des taux de mélange réduits dans les écoulements recouverts de glace comparés aux écoulements à surface libre. Cependant, les résultats dus à l'utilisation d'une injection du type jet ont donné environ les mêmes concentrations dans les deux cas, indiquant que les effets du mélange par jet compensent la différence de diffusivite.

EFFECT OF ICE COVER ON STREAM FLOWS AND VERTICAL MIXING

By Y. L. Lau[1] and B. G. Krishnappan[2]

INTRODUCTION

The presence of ice cover in a stream alters the flow characteristics to a great extent. The normal flow depth increases due to the increased resistance resulting from an additional solid boundary and the average flow velocity decreases. In addition, both the velocity and shear stress distributions change. Therefore, one can expect differences in the momentum and mass transfer coefficients between the ice-covered stream flows and the open-water stream flows.

In analyzing the vertical mixing processes in channel flows, it is customary to assume that the mass transfer coefficient in the vertical direction (Γ_y) is directly proportional to the turbulent kinematic viscosity (ν_t) which can be evaluated from the shear stress distribution τ (y) and the velocity distribution u(y) using the Boussinesq hypothesis. With this assumption, Γ_y can be calculated from the following equation:

$$\Gamma_y = \frac{\nu_t}{\sigma_\phi} = \frac{1}{\sigma_\phi} \left(\frac{\tau/\rho}{\partial u/\partial y} \right) \qquad (1)$$

where σ_ϕ is a proportionality constant and ρ is the density of the fluid.

---

[1]Head, Environmental Hydraulics Section, Hydraulics Research Division, National Water Research Institute, Canada Centre for Inland Waters, Burlington, Ontario, Canada, L7R 4A6.

[2]Research Scientist, Environmental Hydraulics Section, Hydraulics Research Division, National Water Research Institute, Canada Centre for Inland Waters, Burlington, Ontario, Canada, L7R 4A6.

For a two-dimensional, fully developed turbulent flow in an open channel with free surface, for which linear shear stress and logarithmic velocity distributions are often used, Eq. 1 gives a parabolic distribution for Γ_y with Γ_y being maximum at mid-depth and zero at the stream bed and at the free surface.

In analyzing the flow structure in an ice-covered stream, the flow is usually divided into two layers, separated by the line of maximum velocity, with linear shear stress and logarithmic velocity distributions within each layer (3, 4, 10, 12). However, these distributions lead to parabolic distributions of ν_t and Γ_y in each layer with a value of zero at the location of maximum velocity as shown in Fig. This is obviously incorrect because it implies no momentum or mass transfer across the plane of maximum velocity. To avoid this obvious deficiency, the distribution of Γ_y may be arbitrarily altered as by Shen and Harden (10) who adopted the assumption that Γ_y is constant in the central portion of the flow, as suggested by Ismail (1). The assumed profile is shown in Fig. 1.

In addition to the arbitrary modification of the Γ_y distribution, Shen and Harden had to assume that the depth remains constant when the flow acquires an ice cover. This is also not correct because, given the same discharge, the depth will increase with the presence of an ice cover. In this paper, an alternate approach has been adopted to overcome the above difficulties. The "k-ε" turbulence model, described in detail by Launder and Spalding (5), is used to calculate the depth, velocity distribution and ν_t distribution for two flows with the same given discharge, bed slope and bottom roughness. One of these flows has a free surface at the top while the other has an ice cover of a given roughness. These results are then used in the two-dimensional mass transport equation to simulate the concentration distributions due to sources placed at different heights in the flow. The results give some indications of the effects of ice cover on the flow and on the vertical mixing.

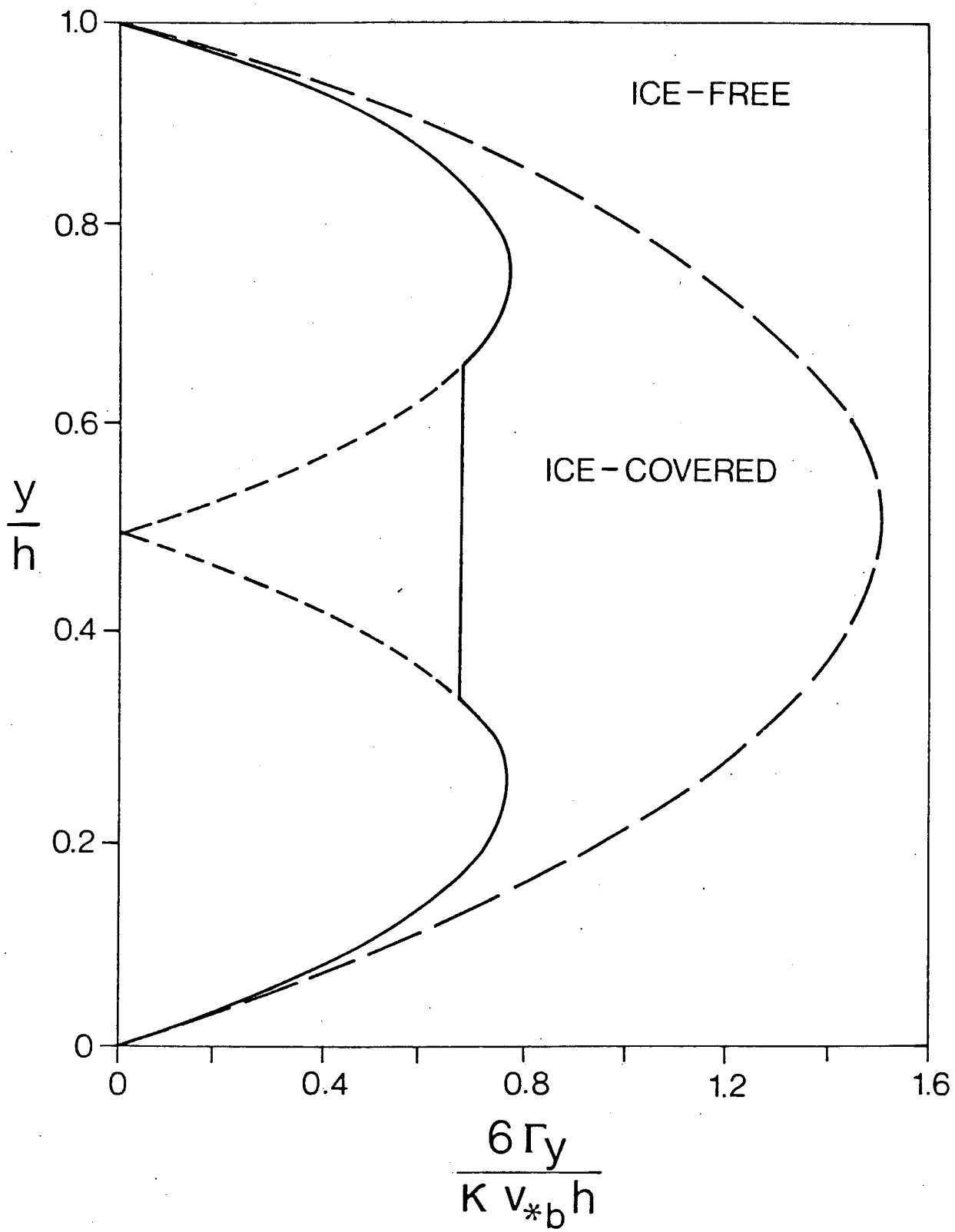

FIGURE 1. COMPARISON OF TRANSFER COEFFICIENTS

THEORETICAL CONSIDERATIONS

In k-ε model of turbulence, the turbulence structure is considered to be governed by two characteristic parameters, namely, the kinetic energy of turbulent motion (k) and its rate of dissipation ε. As a result, the turbulent kinematic viscosity ν_t can be expressed as:

$$\nu_t = c_\mu \frac{k^2}{\varepsilon} \tag{2}$$

in which c_μ is an empirical constant.

Equation 2 permits the evaluation of the ν_t distribution from the distributions of k and ε. The distributions of k and ε, in turn, are determined by solving the semi-empirical transport equations for k and ε along with the continuity and momentum equations for the flow field.

GOVERNING EQUATIONS

For a two-dimensional channel flow, the equations of continuity, momentum and the transport equations for k and ε take the following forms:

$$\frac{\partial u}{\partial x} + \frac{\partial v}{\partial y} = 0 \tag{3}$$

$$\frac{\partial u^2}{\partial x} + \frac{\partial uv}{\partial y} = \frac{\partial}{\partial y}\left(\nu_t \frac{\partial u}{\partial y}\right) + gS \tag{4}$$

$$\frac{\partial uk}{\partial x} + \frac{\partial vk}{\partial y} = \frac{\partial}{\partial y}\left(\frac{\nu_t}{\sigma_k} \frac{\partial k}{\partial y}\right) + G - \varepsilon \tag{5}$$

$$\frac{\partial u\varepsilon}{\partial x} + \frac{\partial v\varepsilon}{\partial y} = \frac{\partial}{\partial y}\left(\frac{\nu_t}{\sigma_\varepsilon} \frac{\partial \varepsilon}{\partial y}\right) + c_1 \frac{\varepsilon}{k} G - c_2 \frac{\varepsilon^2}{k} \tag{6}$$

$$\frac{\partial u\phi}{\partial x} + \frac{\partial v\phi}{\partial y} = \frac{\partial}{\partial y}\left(\frac{\nu_t}{\sigma_\phi} \frac{\partial \phi}{\partial y}\right) + s_\phi \tag{7}$$

The coordinate system chosen is shown in Fig. 2. x axis is measured along the channel bed and y axis is measured perpendicular to x axis in the vertical plane. u, v are the velocity components in x and y directions respectively. S is the slope of the channel bed. $\sigma_k, \sigma_\varepsilon, \sigma_\phi, c_1$ and c_2 are empirical constants. G is the turbulent energy production due to mean motion given by:

$$G = \nu_t \left[\left(\frac{\partial u}{\partial y} \right)^2 + 2 \left(\frac{\partial v}{\partial y} \right)^2 \right] \tag{8}$$

ϕ is a scalar quantity such as temperature in the case of heat transfer problem and concentration in the case of mass transfer. s_ϕ is the volumetric source rate of ϕ.

The empirical constants were determined by Launder and Spalding (5) who considered a variety of flows such as flows in pipes, channels, mixing layers, jets and wakes. The values arrived at by Launder and Spalding are:

$$\left.\begin{aligned} c_\mu &= 0.09 \\ \sigma_k &= 1.00 \\ \sigma_\varepsilon &= 1.30 \\ c_1 &= 1.43 \\ c_2 &= 1.92 \\ \sigma_\phi &= \begin{cases} 1.00 \text{ for mass transfer} \\ 0.50 \text{ for heat transfer} \end{cases} \end{aligned}\right\} \tag{9}$$

The governing equations listed above are derived with the assumption that the flow is predominantly in one direction, namely, along x and the turbulent transport of u, k, ε and ϕ is negligible in that direction, i.e., the terms containing the second order derivatives in x are <u>not</u> included in the set of equations. This assumption helps to modify the type of the equations, i.e. it changes the equations from elliptic type to parobolic type. The parabolic type of equation is especially suitable for numerical schemes which solve the equations

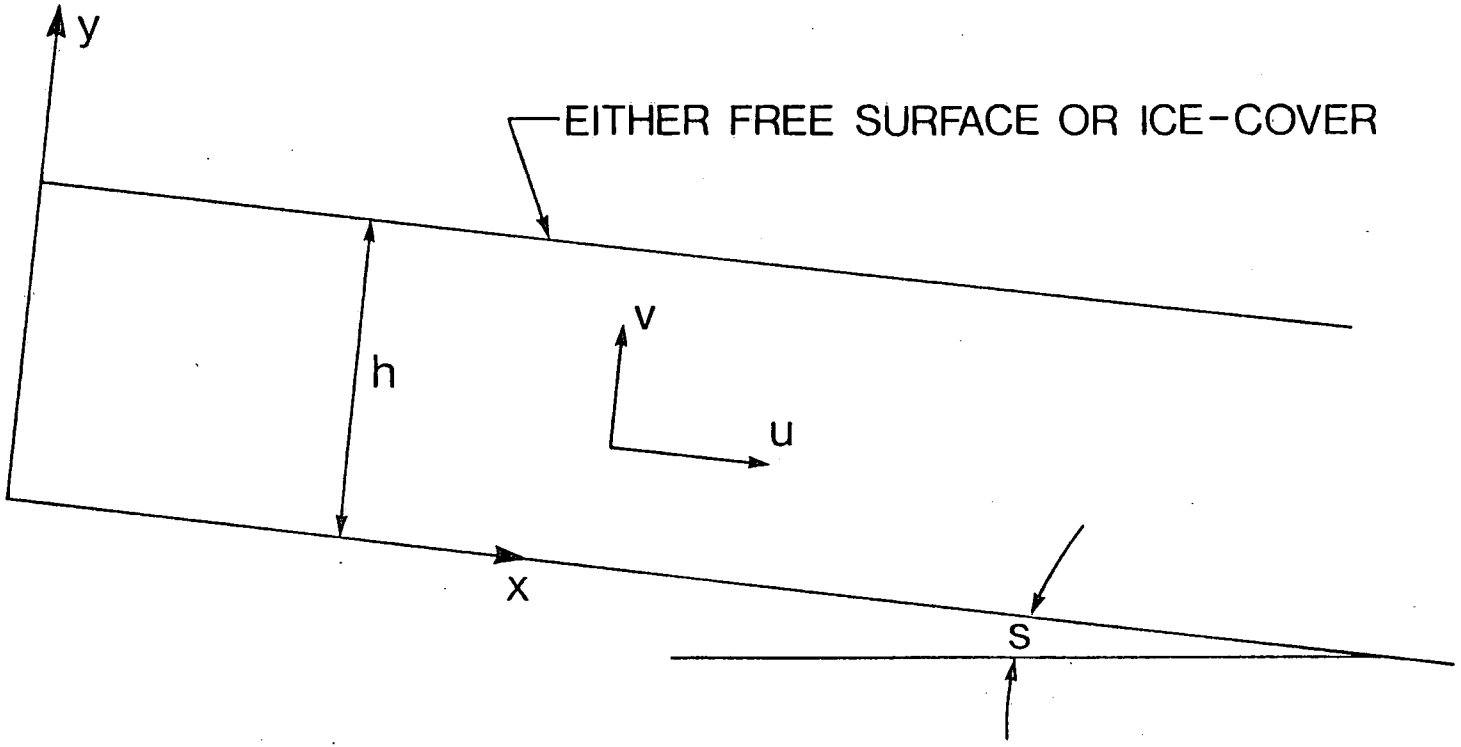

FIGURE 2. CO-ORDINATE SYSTEM

for one station at a time and march forward along x. Such numerical schemes require less computer memory and are executed at a much faster rate.

The fully developed distributions of velocity and turbulent kinematic viscosity which are required for evaluating the effects of ice cover on the flow and mixing characteristics are obtained as asymptotic distributions resulting from the solution of the governing equations. The same results could have been obtained by solving a set of ordinary differential equations representing the fully developed flows. Indeed, for fully developed flows, the variation of flow properties along x vanishes and hence the governing equations are simplified as:

$$\left.\begin{aligned} \frac{d}{dy}\left(\nu_t \frac{du}{dy}\right) &= -gS \\ \frac{d}{dy}\left(\frac{\nu_t}{\sigma_k} \frac{dk}{dy}\right) &= \varepsilon - G \\ \frac{d}{dy}\left(\frac{\nu_t}{\sigma_\varepsilon} \frac{d\varepsilon}{dy}\right) &= c_2 \frac{\varepsilon^2}{k} - c_1 \frac{\varepsilon}{k} G \end{aligned}\right\} \qquad (10)$$

The numerical schemes to solve such a system of ordinary differential equations might have been simpler in comparison to those required to solve the partial differential equations. However, the prediction of concentration distributions, still requires the solution of the partial differential equation, i.e. Eq. 7. In addition, this approach also enables the investigation of jet type discharges. Therefore, it was decided to solve the governing equations as expressed by Eqs. 3 to 6 rather than the set given by Eq. 10.

BOUNDARY CONDITIONS

Equations 2 to 7 form a closed set of equations with the values of empirical constants as given by Eq. 9 and hence can be solved simultaneously for u, v, k, ε,

ν_t and ϕ. Boundary conditions for the above parameters have to be specified:

1) at the channel bed, i.e. at y=0 for all x.

2) at the upper boundary, i.e. at y=h for all x.

3) at the initial cross section, i.e. at x=0 for all y (initial profiles).

Because of the parabolic nature of the governing equations, the boundary conditions at the downstream end of the calculation domain need not be specified. The boundary conditions adopted for the present calculations are similar to those used by Rastogi and Rodi (7), except for the condition for ε at the free surface.

Boundary Conditions at Solid Boundaries. - For the boundary layer type of flows considered, the longitudinal velocity component near the channel bed, and near the ice cover obeys the universal law of the wall i.e., the velocity component u has to satisfy

$$\frac{u_w}{v_*} = \frac{1}{\kappa} \ln \left(E \frac{v_* y_w}{\nu} \right) \qquad (11)$$

where v_* is the shear velocity defined in terms of boundary shear stress τ_b and the fluid density ρ as

$$v_* = \sqrt{\tau_b/\rho} \qquad (12)$$

κ is the Von-Karman constant, equal to 0.42, ν is the kinematic viscosity of the fluid, E is a roughness parameter which takes a value of 9.0 for hydraulically smooth turbulent flows and $(30.1/\frac{v_* K_s}{\nu})$ for rough turbulent flows and y_w is the distance from the solid boundary of a grid point nearest to the solid boundary.

The symbol, K_s, represents the size of the equivalent sand grain roughness for the solid boundary.

The vertical velocity component v at the solid boundaries is zero.

The turbulent kinetic energy k and its dissipation rate ε near solid boundaries are evaluated using the following assumptions:

1) near the solid boundaries, the production of turbulent kinetic energy is equal to the rate of dissipation.

   i.e. $G = \varepsilon$

2) the turbulent shear stress τ near the solid boundary is constant and is equal to the boundary shear stress.

   i.e. $\tau = \tau_b$

3) the velocity distribution in the vicinity of the solid boundary is given by Eq. 11).

Under these conditions, the kinetic energy of turbulence and its dissipation rate near the solid boundaries can be evaluated as:

$$\left.\begin{aligned} k_w &= \frac{v_*^2}{\sqrt{c_\mu}} \\ \varepsilon_w &= \frac{v_*^3}{\kappa\, y_w} \end{aligned}\right\} \qquad (13)$$

For heat and/or mass transfer, the flux at the solid boundaries is assumed to be zero.

Boundary Conditions at the Free Surface. - Following the approach adopted by Rastogi and Rodi (8), the free surface is treated as a symmetry plane for u, k and ϕ. Accordingly, the y gradients for u, k and ϕ become zero. For ε, a condition similar to that at the solid boundary is used to account for the

reduction of the turbulent length scale in the vicinity of the free surface. This condition is expressed as:

$$\varepsilon_f = \frac{(k_f \sqrt{c\mu})^{3/2}}{\kappa\, y_f} \qquad (14)$$

where k_f is the turbulent kinetic energy at the free surface calculated using the symmetry boundary condition and y_f is the distance of the nearest grid point from the free surface. The vertical velocity component v at the free surface is zero.

Initial Profiles. - At the starting cross-section i.e. at x=0, the distributions of u, v, k, ε and ϕ are not known a priori, certain assumptions have to be made in specifying them. The distributions used in the present work are outlined below:

1. Free surface flow case: The velocity component u follows logarithmic distribution in the vicinity of the channel bed; i.e. Eq. 11. In the remaining part of the flow region a uniform distribution is assumed. The assumed distribution has to satisfy the requirement that it yields the specified flow rate per unit width of the channel. The distributions for k and ε are assumed to be uniform over the whole height of the flow field with values k_w and ε_w evaluated from Eq. 13. The vertical velocity component v is assumed to be zero everywhere. The profile for ϕ is assumed to be uniform over the outfall thickness.

2. Ice-covered flow case: The velocity component u follows logarithmic distribution both near the channel bed and near the ice cover. In the central region of the flow, u is assumed to be uniform. Here again, the assumed distribution has to yield the specified flow rate per unit width of channel. Linear profiles for k and ε are used with the values k_w and ε_w evaluated both at channel bed and at ice cover using Eq. 13. The vertical velocity component v is zero everywhere and uniform profile for ϕ is used over the outfall thickness.

NUMERICAL SCHEME

For the present work, the numerical scheme proposed by Patankar and Spalding (6) is adopted. For the sake of completeness, some of the salient features of the numerical scheme are presented in this paper. The forms of Eqs. 4, 5, 6 and 7 are such that one single numerical scheme can be used to solve all the equations. Indeed, Eqs. 4, 5 and 6 can be expressed in the form of Eq. 7. As an example, Eq. 4 is identical to Eq. 7 when u is equated to ϕ and gS to s_ϕ. Therefore, in presenting the details of the numerical scheme here, only Eq. 7 is considered.

In the scheme proposed by Patankar and Spalding the finite difference equations of the differential Eq. 7 are arrived at by integrating the differential equation term by term over small control volumes. Certain assumptions need to be made regarding the variation of ϕ along x and y directions. Referring to Fig. 3a, I is the upstream grid line where the solution for ϕ is known and I+1 is the downstream grid line located at a distance Δx from the upstream grid line where the values of ϕ are to be determined. J-1, J and J+1 are the grid points in the y direction. J+1/2 and J-1/2 are the mid points between J and J+1 and J and J-1 respectively. The control volume over which the equation is integrated is shown by hash lines. The variation of ϕ in the y direction is assumed to be linear between grid points as shown in Fig. 3b. The variation of ϕ along x is assumed to be stepwise, being uniform and equal to the value corresponding to the downstream grid. The step change occurs right at the upstream grid line. Such an assumption of ϕ along x gives rise to implicit form of finite difference equations.

When each term of the differential Eq. 7 is integrated over the control volume shown in Fig. 3a and substituted back in the equation the following relation is obtained:

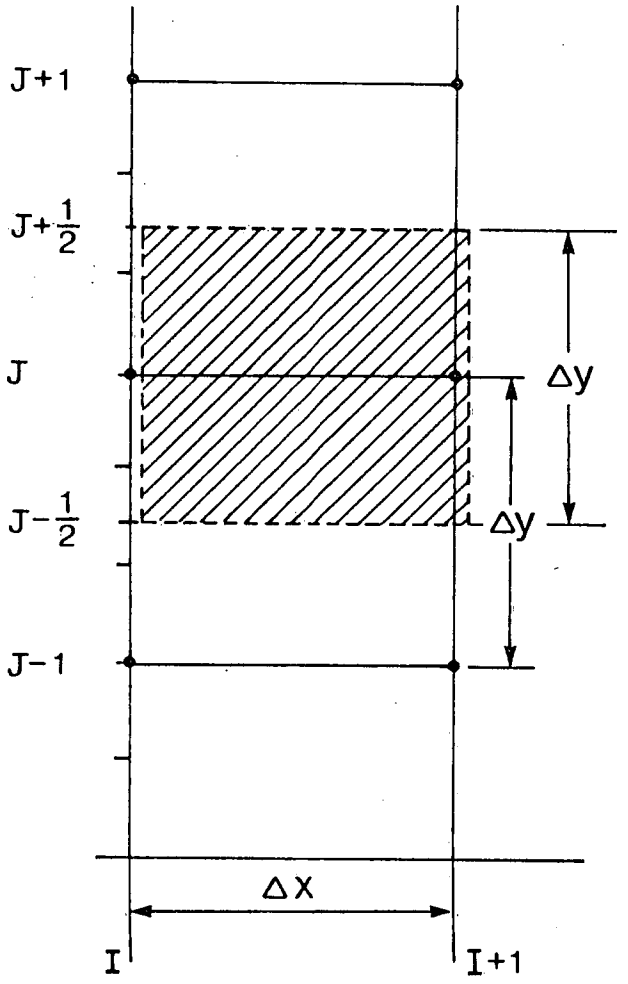

FIGURE 3a. CONTROL VOLUME

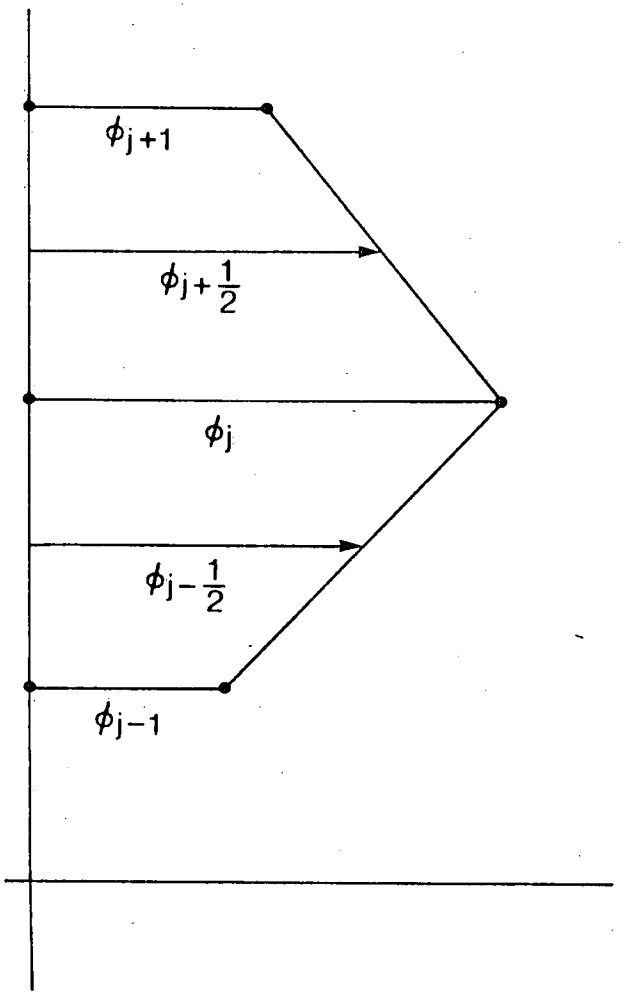

FIGURE 3b. ASSUMED PROFILE FOR ϕ IN y DIRECTION BETWEEN GRID POINT

$$\{\tfrac{3}{4}(P+\Omega)_J\,\Delta y + L_{J+1/2} - L_{J-1/2} + 2T_{J+1/2} + 2T_{J-1/2} - s\}\,\phi_J +$$

$$\{\tfrac{1}{8}(P+\Omega)_J\,\Delta y + L_{J+1/2} - 2T_{J+1/2}\}\,\phi_{J+1} +$$

$$\{\tfrac{1}{8}(P+\Omega)_J\,\Delta y - L_{J-1/2} - 2T_{J-1/2}\}\,\phi_{J-1} =$$

$$\{\tfrac{1}{4}\,P_J(3\,\phi_I\,\Delta y + \phi_{I,J+1}\,\tfrac{\Delta y}{2} + \phi_{I,J-1}\,\tfrac{\Delta y}{2}) + 2s_I\} \qquad (15)$$

where $P_J = \dfrac{u_{I,J}}{\Delta x}$

$\Omega_J = \dfrac{1}{\Delta y}(L_{J-1/2} - L_{J+1/2})$

$L_{J-1/2} = v_{J-1/2}$

$L_{J+1/2} = v_{J+1/2}$

$T_{J+1/2} = \dfrac{2(\nu_t/\sigma_\phi)_{J+1/2}}{\Delta y}$

$T_{J-1/2} = \dfrac{2(\nu_t/\sigma_\phi)_{j-1/2}}{\Delta y}$

s and s_I result from the integration of the source term s_ϕ over the control volume and their values depend on the entity which ϕ represents. In Eq. 15, all the terms except the ones with s_I and ϕ_I represent the values at the downstream grid line I+1. (The subscript (I+1) is omitted for ease of writing. When Eq. 15 is written out for all values of J, a series of finite difference equation results which can be expressed as a tri-diagonal matrix equation. There are several standard methods to solve such a system of algebraic equations. In the present calculations a simple successive-substitution formulae proposed by Patankar and Spalding were used.

APPLICATION OF THE NUMERICAL SCHEME

In order to evaluate the effects of ice cover on the flow properties and the vertical mixing characteristics in channel flows, it is necessary to solve the governing equations for both free surface case and the ice cover case. For these two flows to be equivalent, it is assumed that both channels carry the same flow rate, have the same bottom slope and the same bottom roughness elements. The flow depths, of course, will be different. The flow depth in the ice-covered flow will be larger than that of the free surface flow because of the increased resistance due to the ice cover. Since the flow depths are not known a priori, a trial and error method is required. The procedure adopted in the present work is illustrated step by step in the following.

CALCULATIONS FOR FREE-SURFACE FLOW

Step 1 The values of flow rate per unit width q and the channel bed roughness K_s are assumed to be specified. A value for the flow depth h_o is selected. (Subscript o is used to denote free-surface flow properties and i is used for ice-covered flow properties.)

Step 2 Using this flow depth, a numerical grid is laid in the x-y plane as shown in Fig. 4a.

Step 3 An initial velocity profile $u_o(y)$ at the starting grid line (at x=0) is assumed as outlined earlier. This profile has to satisfy the condition:

$$\int_0^{h_o} u_o(y)\, dy = q$$

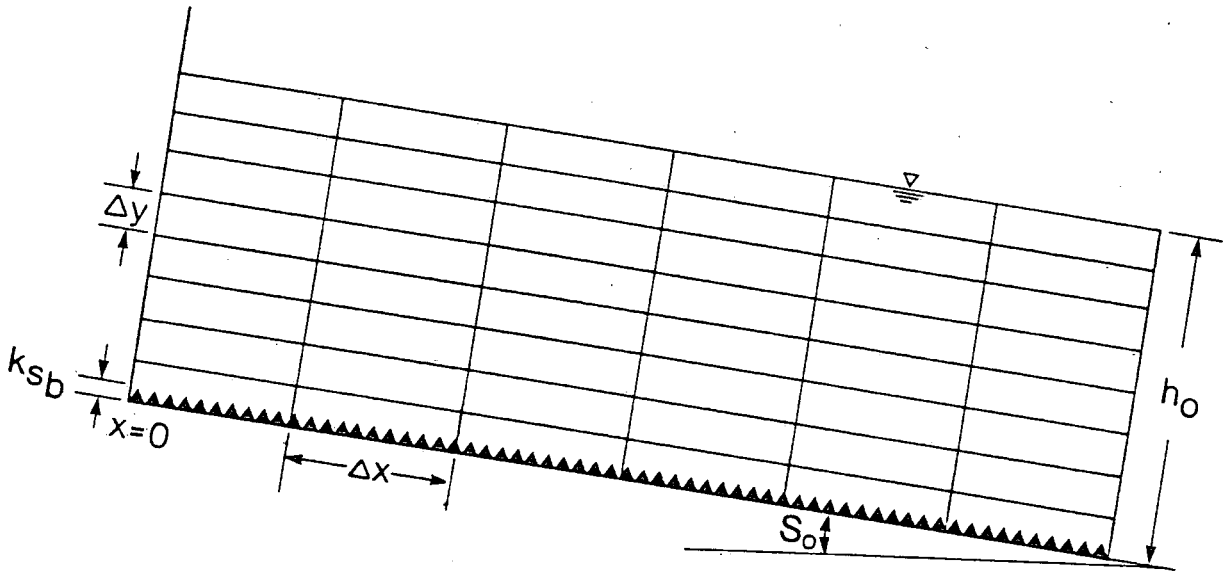

FIGURE 4a. NUMERICAL GRID FOR FREE SURFACE FLOW COMPUTATIONS

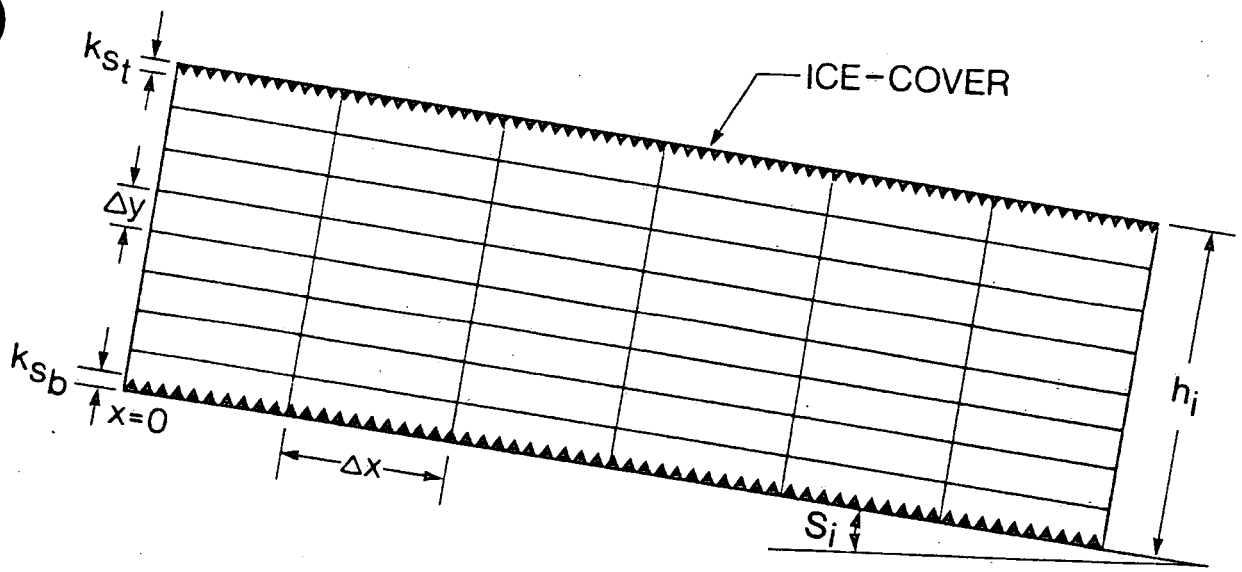

FIGURE 4b. NUMERICAL GRID FOR ICE-COVER FLOW COMPUTATIONS

Step 4 From the inital profile for u_o, the shear velocity v_* is evaluated using Eq. 11.

Step 5 Knowing v_*, the boundary values for k and ϵ are evaluated using Eq. 13 and uniform distributions for k and ϵ are assumed along the first grid line (at x =0).

Step 6 Knowing k and ϵ distributions, the distribution for turbulent kinematic viscosity ν_t is obtained using Eq. 2.

Step 7 Knowing ν_t and initial profile for u, the momentum equation is solved using the numerical scheme and the velocity profile at the downstream station at $x=\Delta x$ is obtained. The value of slope S appearing in the equation is evaluated as follows:

$$S_o = \frac{v_*^2}{gh_o} \tag{16}$$

Step 8 Knowing u_o at x=0 and u_o at $x=\Delta x$, the continuity Eq. 3 is solved to obtain the vertical velocity component v_o.

Step 9 From the velocity profile at $x=\Delta x$, shear velocity v_* is computed for the grid line at $x=\Delta x$ and the boundary values for k and ϵ at $x=\Delta x$ are evaluated.

Step 10 The equations for k and ϵ are then solved to obtain k and ϵ profiles along the grid line at $x=\Delta x$.

Step 11 Knowing k and ϵ profiles, the ν_t distribution at $x=\Delta x$ is computed.

Step 12 The steps 7 to 11 are then repeated several times until a certain downstream distance $x = X_o$ is reached where the profiles of u and ν_t no longer change from grid line to grid line, i.e. where the profiles become fully developed. At this point, the vertical velocity component is zero and the value of slope S_o computed using Eq. 16 becomes invariant with respect to x. Therefore, for the specified flow rate per unit width q and the bed roughness K_s, the free surface

flow with bed slope S_o will flow at a uniform depth of h_o. This completes the calculations for open water flow.

CALCULATIONS FOR ICE-COVERED FLOW

Step 1 The values of flow rate per unit width of channel and the channel bed roughness for the flow under ice cover are the same as for the free surface flow calculated above.

The roughness of the ice-cover surface has to be specified. Let it be K_{s_t}. The bed roughness for the ice-covered channel is denoted by K_{s_b} and its value is equal to K_s. A value for the flow depth h_i is selected.

Step 2 Using the flow depth h_i, a numerical grid is laid in the x-y plane as shown in Fig. 4b.

Step 3 An initial velocity profile $u_i(y)$ at the starting grid line (at x=0) is assumed as outlined earlier. The initial velocity profile has to satisfy the condition:

$$\int_0^{h_i} u_i(y)\, dy = q$$

Step 4 From the initial profile $u_i(y)$, the shear velocities at the channel bed and at the ice cover, v_{*b} and v_{*t}, were calculated using Eq. 11.

Step 5: Knowing v_{*b} and v_{*t}, the boundary values for k and ϵ are evaluated using Eq. 13 and linear distributions for k and ϵ are assumed along the first grid line (at x=0).

Step 6 Knowing k and ϵ distributions, the distribution for ν_t is obtained using Eq. 2.

Step 7 Knowing ν_t and initial profile u_i, the momentum equation is solved using the numerical scheme and the velocity profile at the downstream station at $x=\Delta x$ is obtained. The value of the slope S appearing in the equation is evaluated as:

$$S_i = \left(\frac{v_{*b}^2 + v_{*t}^2}{gh_i}\right) \qquad (17)$$

Step 8 Knowing u_i at $x=0$ and u_i at $x=\Delta x$, the continuity Eq. 3 is solved to obtain the vertical velocity component v_i.

Step 9 From the velocity profile at $x=\Delta x$, shear velocities v_{*b} and v_{*t} are computed for the grid line at $x=\Delta x$ and the boundary values for k and ε at $x=\Delta x$ are evaluated.

Step 10 The equations for k and ε are then solved to obtain k and ε profiles along the grid line at $x=\Delta x$.

Step 11 Knowing k and ε profiles, ν_t profile at $x=\Delta x$ is computed.

Step 12 Steps 7 to 11 are repeated several times until a certain downstream distance $x=X_i$ is reached where the profiles of u and ν_t no longer change from grid line to grid line, i.e. where the profiles become fully developed. At this stage, the vertical velocity component v_i is zero and the shear velocities v_{*b} and v_{*t} become invariant with respect to x. Consequently, the slope S_i computed using Eq. 17 is also invariant with respect to x. For the specified flow rate q, bed roughness k_{s_b} and ice-cover roughness k_{s_t}, the ice-covered flow becomes uniform with depth h_i for the slope S_i. Now, if this slope S_i is not the same as the slope S_o of the uniform free surface flow, previously computed, then a different value for h_i is selected and the calculations in steps from 2 to 12 are repeated until S_i coincides with S_o. The flow depth h_i corresponding to this slope then yields an equivalent ice-covered flow to the free-surface flow.

RESULTS AND DISCUSSIONS

Using the procedure outlined in the last section, fully developed profiles of u and ν_t were obtained for three different flow conditions in both free-surface and ice-covered channels. The hydraulic parameters for the three flow conditions are shown schematically in Fig. 5 and are also listed in Table 1. In the first flow condition, denoted as run no. 1, value for K_s for both channels was taken as 3 mm. The flow rate per unit width was taken as 2230 cm^2/sec for both channels. The ice cover was considered to act as an hydraulically smooth surface.

In run no. 2, the bed roughness was increased to 5 mm and the ice-cover roughness was kept the same as in run no. 1. In run no 3, the bed roughness was kept the same as run no. 2 and the ice-cover roughness was increased to 5 mm. The resulting flow depths, shear velocities and slopes are listed in Table 1 and are also shown in Fig. 5. As expected, the ice-covered flows required larger flow depths to transport the same flow rate with same bed slope. The increase in flow depth varied from 15 percent to 31 percent. Calculations have also been made for a much deeper flow which resembles closer to a natural flow. In that case, the depth increased from 2.7 m to 3.0 m when an ice cover was present, an increase of 11.1 percent. The shear velocities at the bed of ice-covered flows were smaller than those for the free-surface flows. The latter result indicates that if the bed of the stream is movable, then the sediment transporting capacity would be diminished by the presence of ice cover. Furthermore, the bed forms resulting from the movement of sediment would also be different from the free-surface flows, which in turn could alter the roughness characteristics. Therefore, the presence of ice cover can produce significant changes to the hydraulic characteristics of natural stream flows. However, it should be noted that if the

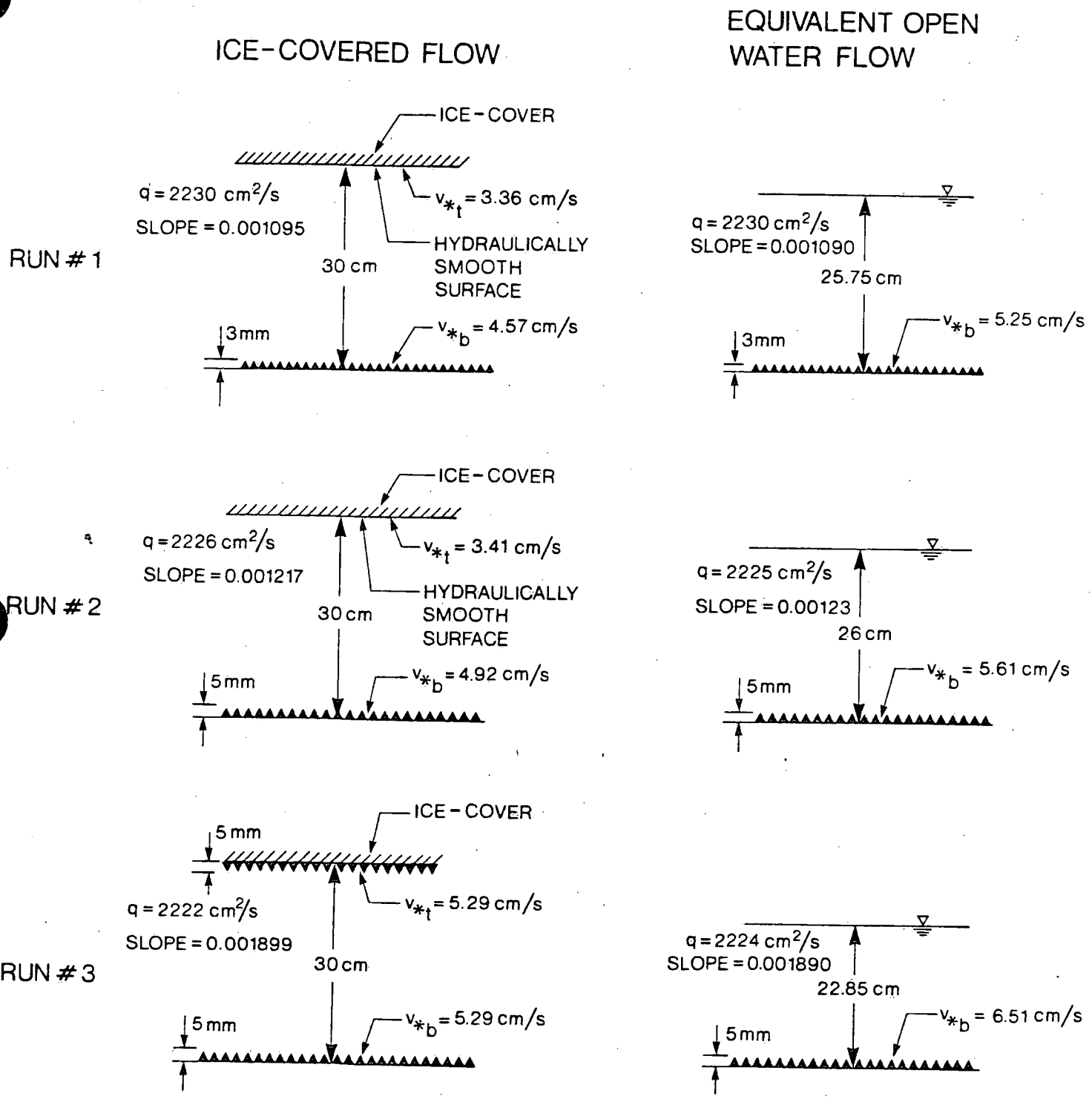

FIGURE 5. SCHEMATIC REPRESENTATION OF THE FLOWS SIMULATED

TABLE 1. - Hydraulic Parameters for the Simulated Runs

Run No.	Run No. 1		Run No. 2		Run No. 3	
Flow Properties	Open Water Flow	Ice-Covered Flow	Open Water Flow	Ice-Covered Flow	Open Water Flow	Ice Covered Flow
(1)	(2)	(3)	(4)	(5)	(6)	(7)
Flow rate per unit width in cm^2/s	2230	2230	2225	2226	2224	2222
Bed roughness k_{s_b} in mm.	3	3	5	5	5	5
Ice-cover roughness k_{s_t} in mm.	N/A	hydraulically smooth ice cover	N/A	hydraulically smooth ice cover	N/A	5
Shear velocity at the bed v_{*_b} cm/s	5.25	4.57	5.61	4.92	6.51	5.29
Shear velocity at ice cover v_{*_t} cm/s	N/A	3.36	N/A	3.41	N/A	5.29
Slope of Channel	0.0011	0.0011	0.0012	0.0012	0.0019	0.0019
Flow depth in cm	25.75	30.0	26.0	30.0	22.8	30.0

ice-covered flow is divided into an upper and a lower layer, the Darcy friction factor associated with the lower layer is actually larger than in the free surface flow, even though the bed shear stress has decreased. This is because the mean velocity in the lower layer has decreased by a proportionately larger amount.

Profiles of u for the three runs are shown in Fig. 6. Solid lines represent the ice-covered flows and the dotted lines denote the free-surface flows. In all three runs, the ice-covered flow velocities are lower than those of the free-surface flows. u profiles in ice-covered flows resemble the ones measured by Larsen (3, 4) with close to zero gradients over substantial portions of the central region. Such profiles mean that the division of the flow into two layers, as has been done by previous investigators, can be very subjective. The u profiles in ice-covered flows are reasonably sensitive to the roughness characteristics of both bed surface and ice-cover surface. When the bed roughness increases in comparison to the ice-cover roughness, the position of maximum velocity moves closer to the smoother surface. The profile becomes symmetrical when the roughness values of bed surface and ice-cover surface are made equal as in run no. 3.

Free-surface u profiles were replotted in Fig. 7 on semi-log axes to check the validity of the logarithmic distribution for u. The profiles are close to being linear for about 75 percent of the flow depth for all three runs, but deviate from linearity, i.e. logarithmic distribution, for the remaining 25 percent near the free surface. This result is in agreement with a recent study by Song and Yang (11) who put forward the hypothesis that the flow in a wide open channel consisted of three different regions, namely, the laminar sublayer region, very close to the channel bed; an inner turbulent region in the middle and an outer turbulent region near the free surface. Based on the experimental work of Vanoni (13) and Sayre (8), Song and Yang argued that the logarithmic velocity distribution was applicable only to the inner turbulent region. For the outer turbulent region, they proposed a parabolic distribution.

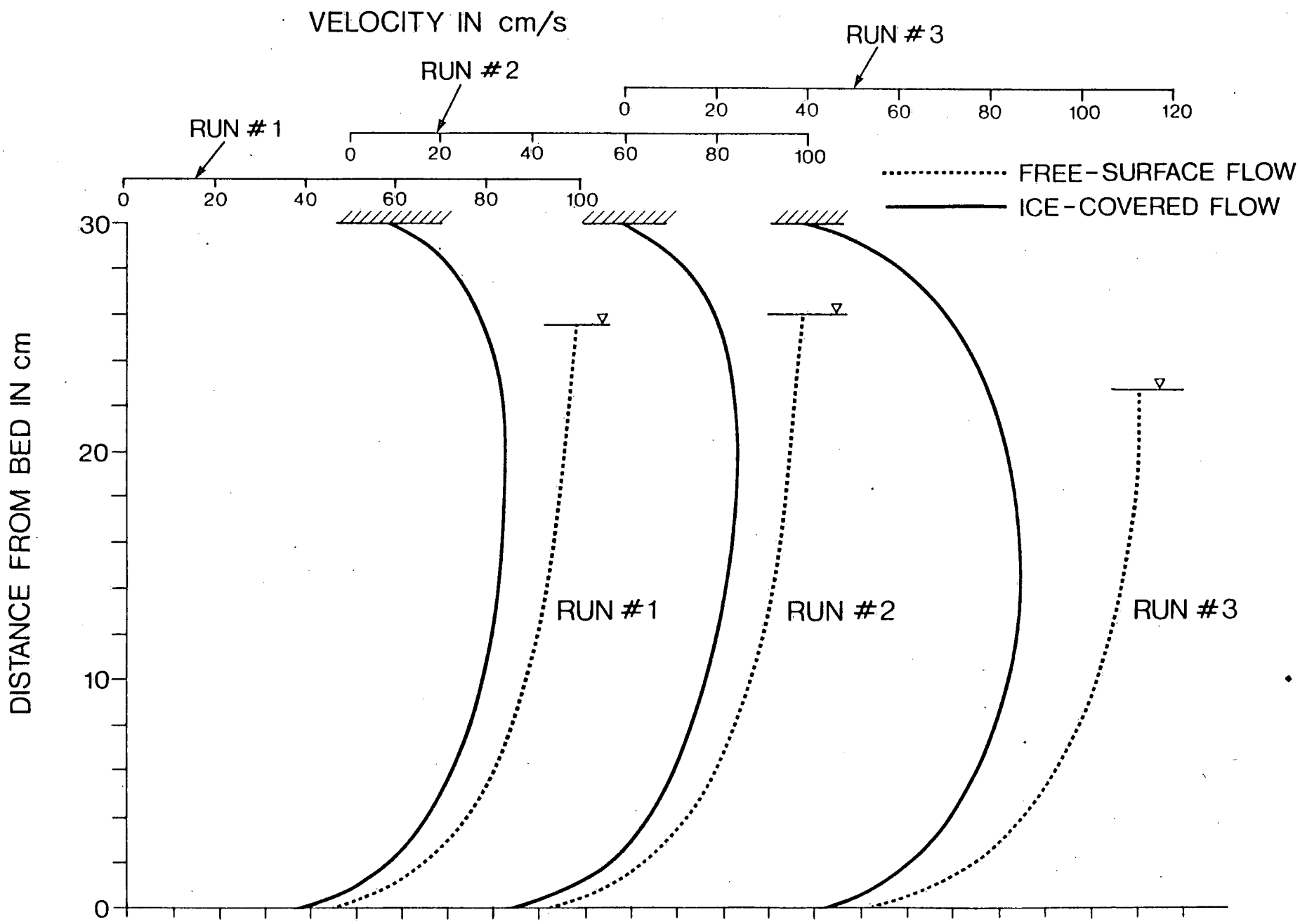

FIGURE 6. VELOCITY DISTRIBUTIONS

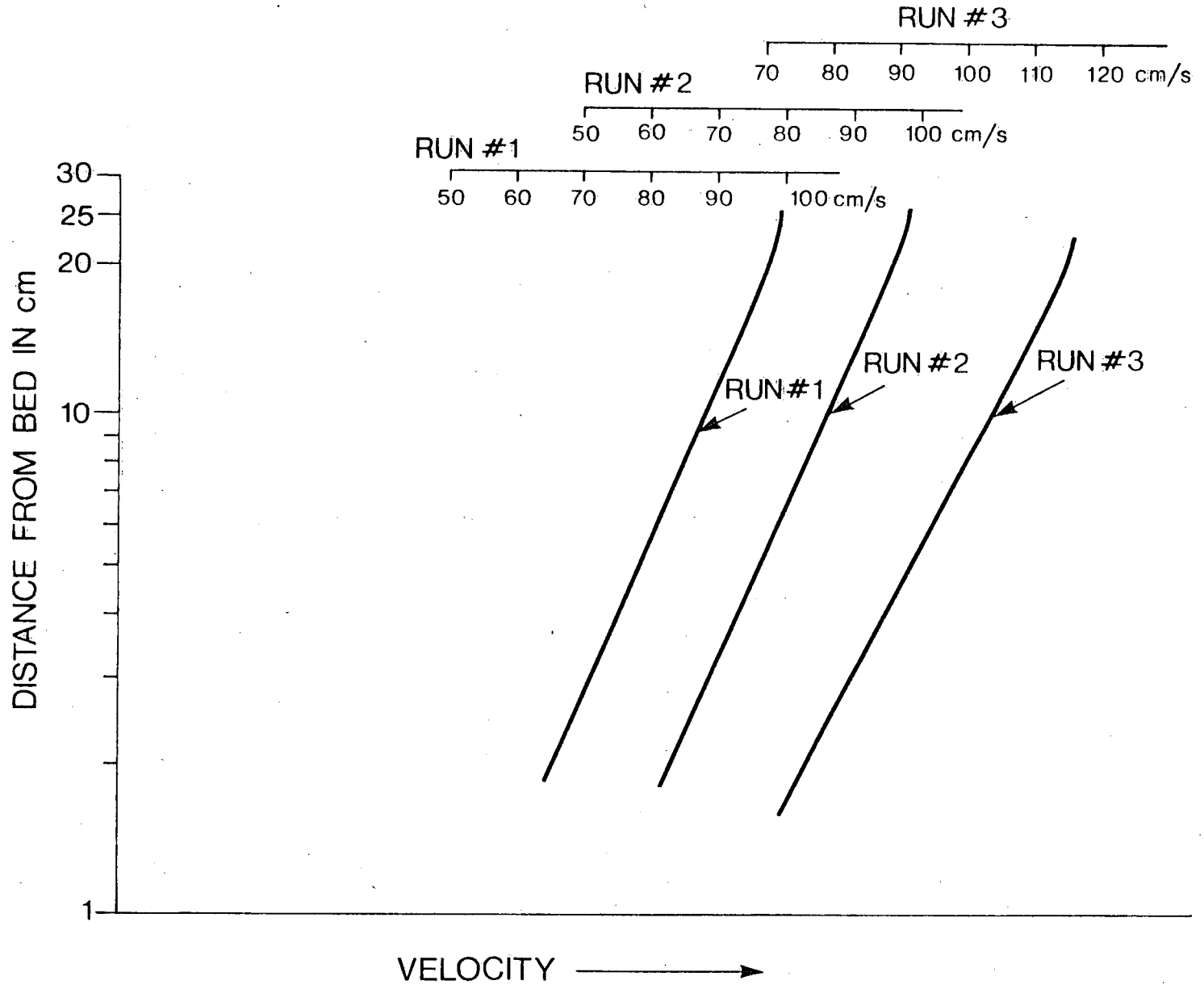

FIGURE 7. VELOCITY DISTRIBUTIONS IN SEMI-LOG PAPER

A parabolic velocity distribution in conjunction with a linear distribution for shear stress would give rise to a constant turbulent kinematic viscosity when the Boussinesq hypothesis is invoked, whereas a logarithmic velocity distribution gives rise to a parabolic distribution for ν_t as shown earlier. Some experiments carried out to measure the turbulent kinematic viscosity (Jobson (2)) do suggest that the ν_t distribution deviates from the parabolic distribution, especially near the free surface which supports the suggestion that the velocity distribution near the free surface indeed is not logarithmic. If it is not logarithmic, then should it be parabolic as Song and Yang suggest The answer to this question is not quite clear. Indeed, the ν_t distributions which are calculated from the k and ϵ distributions using Eq. 2 (shown in Figs. 8a, 8b and 8c) resemble the distribution measured by Jobson and deviate from the parabolic distributions in the upper part of the flow. However, the distributions do not become constant as required for the parabolic velocity distribution.

The ν_t distributions for the ice-covered flows shown in Figs. 8a, 8b and 8c do not suffer from the drawback of having a zero value inside the flow, as in the case when logarithmic velocity and linear shear are assumed for a top and a bottom layer. In fact, Fig. 8c shows that for the case of identical top and bottom roughness ν_t is a maximum at mid-depth.

A comparison between ν_t values for ice-covered flows and free-surface flows indicates that the values for ice-covered flows are smaller than those for the free-surface flows in all three runs. The difference increases as one moves away from the bed. The distributions of ν_t for the ice-covered flows are affected by the relative roughness of the boundaries. For example, in runs no. 1 and 2, the ν_t distributions are skewed towards the rougher lower boundary whereas in run no. 3 for which the roughness values are equal for both boundaries the distribution becomes symmetrical. In the work of Shen and Harden (10) it was assumed that in the central regions of flow the values of ν_t were constant.

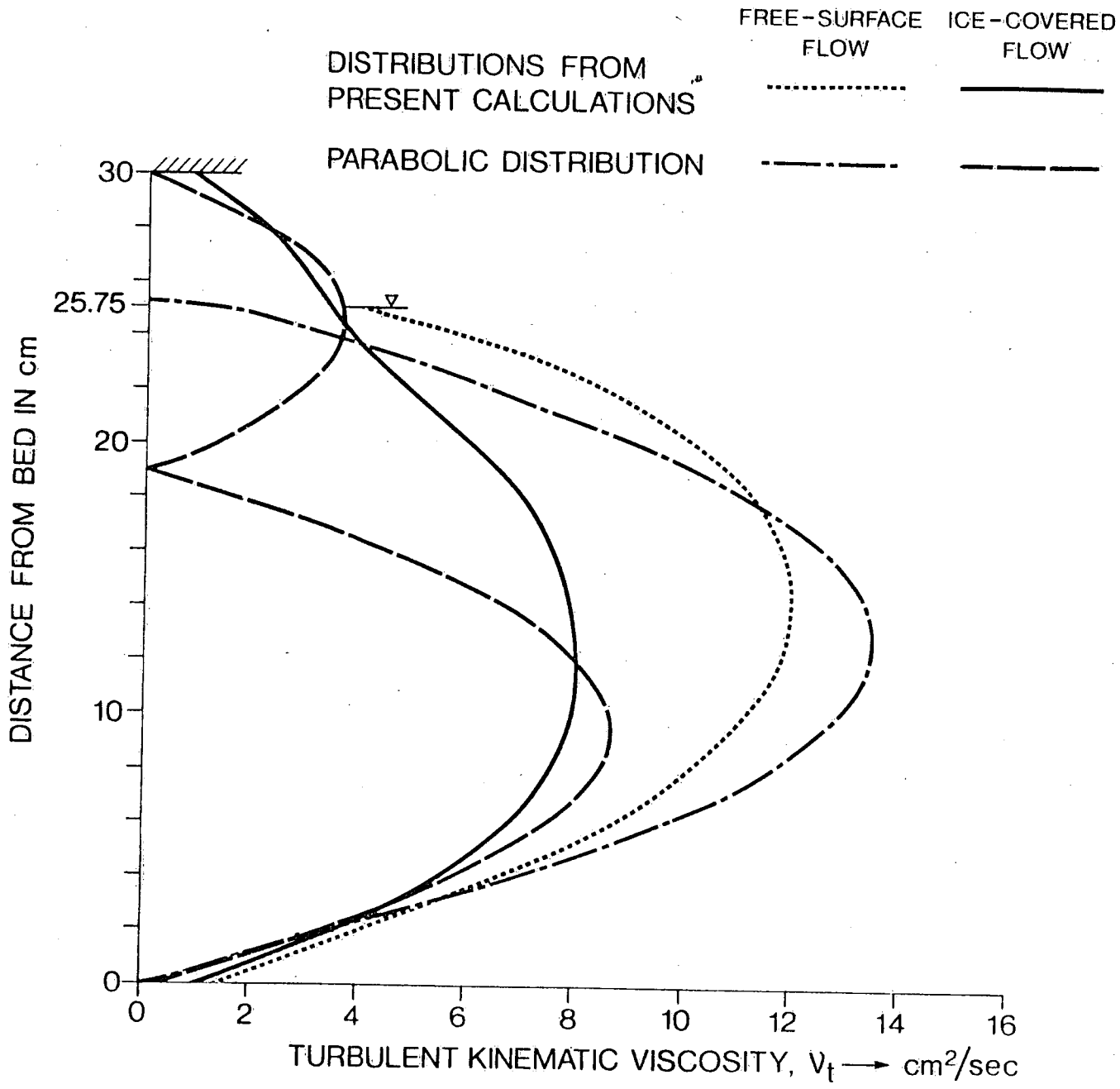

FIGURE 8a. V_t - DISTRIBUTION FOR RUN # 1

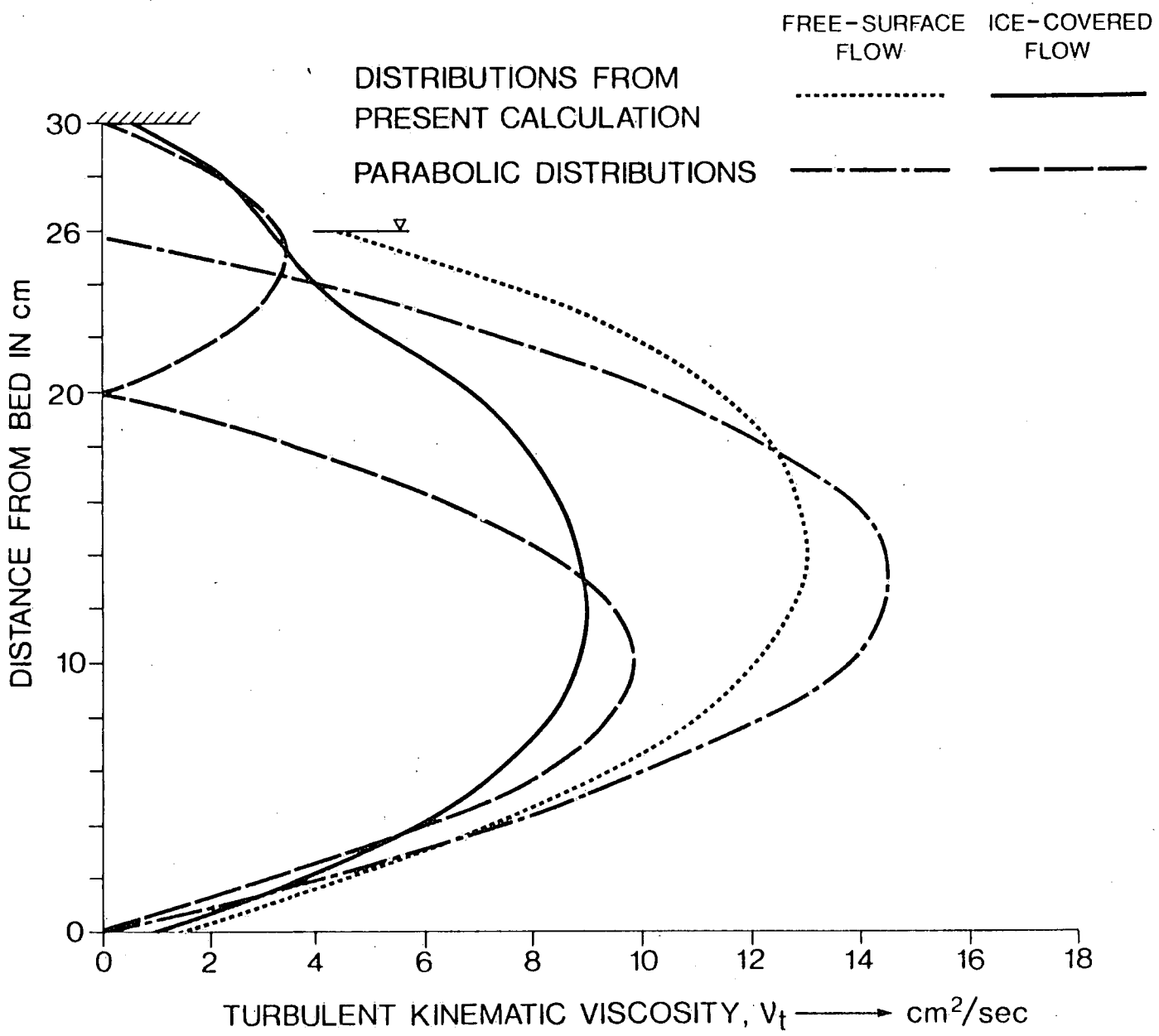

FIGURE 8b. ν_t - DISTRIBUTION FOR RUN # 2

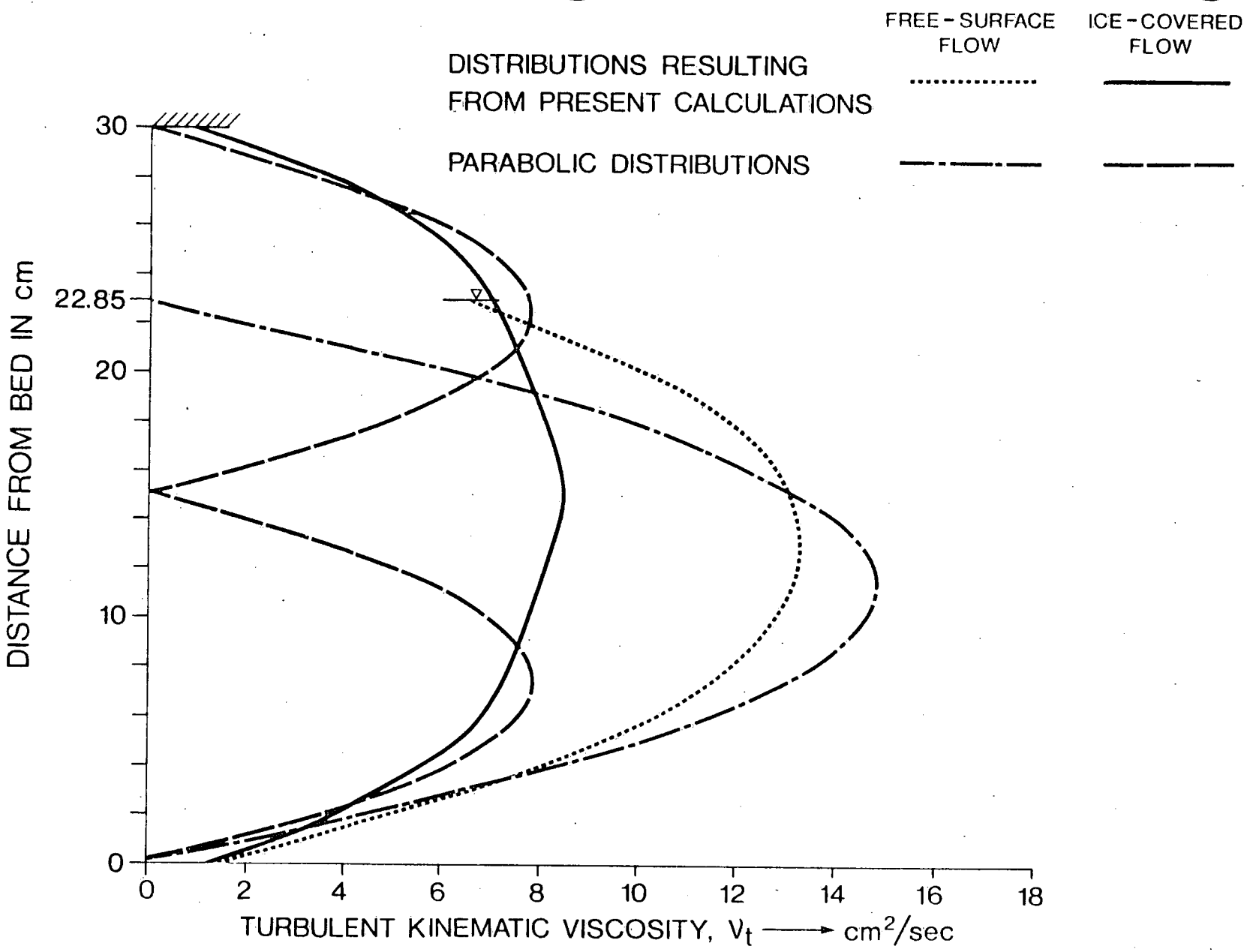

FIGURE 8c. ν_t - DISTRIBUTION FOR RUN # 3

The present calculations show that this is approximatley true only when the roughness values are same for channel bed and ice-cover surface. In cases where the roughness values are different, ν_t values are nowhere near constant even in the central regions.

SHEAR STRESS DISTRIBUTIONS

Using the calculated profiles of u and ν_t, the shear stress distributions $\tau(y)$ were calculated as:

$$\tau(y) = \rho \nu_t \left(\frac{\partial u}{\partial y} \right) \tag{18}$$

The derivative $(\partial u/\partial y)$ was evaluated using a central difference approximation as:

$$\frac{\partial u}{\partial y} = \frac{u_{J+1} - u_{J-1}}{2\Delta y} \tag{19}$$

The resulting shear-stress distributions were plotted in Fig. 9 for all the runs. From Fig. 9 it can be seen that the shear-stress distribution is very close to linear for all the runs. Very close to the solid boundaries, the distributions seem to deviate from the linear profile; this could be due to the approximation involved in calculating the derivative of u as in Eq. 19.

DISTRIBUTION OF A NEUTRALLY BUOYANT TRACER

After calculating the fully developed distributions of u and ν_t, calculations were performed to obtain concentration distributions of a neutrally buoyant

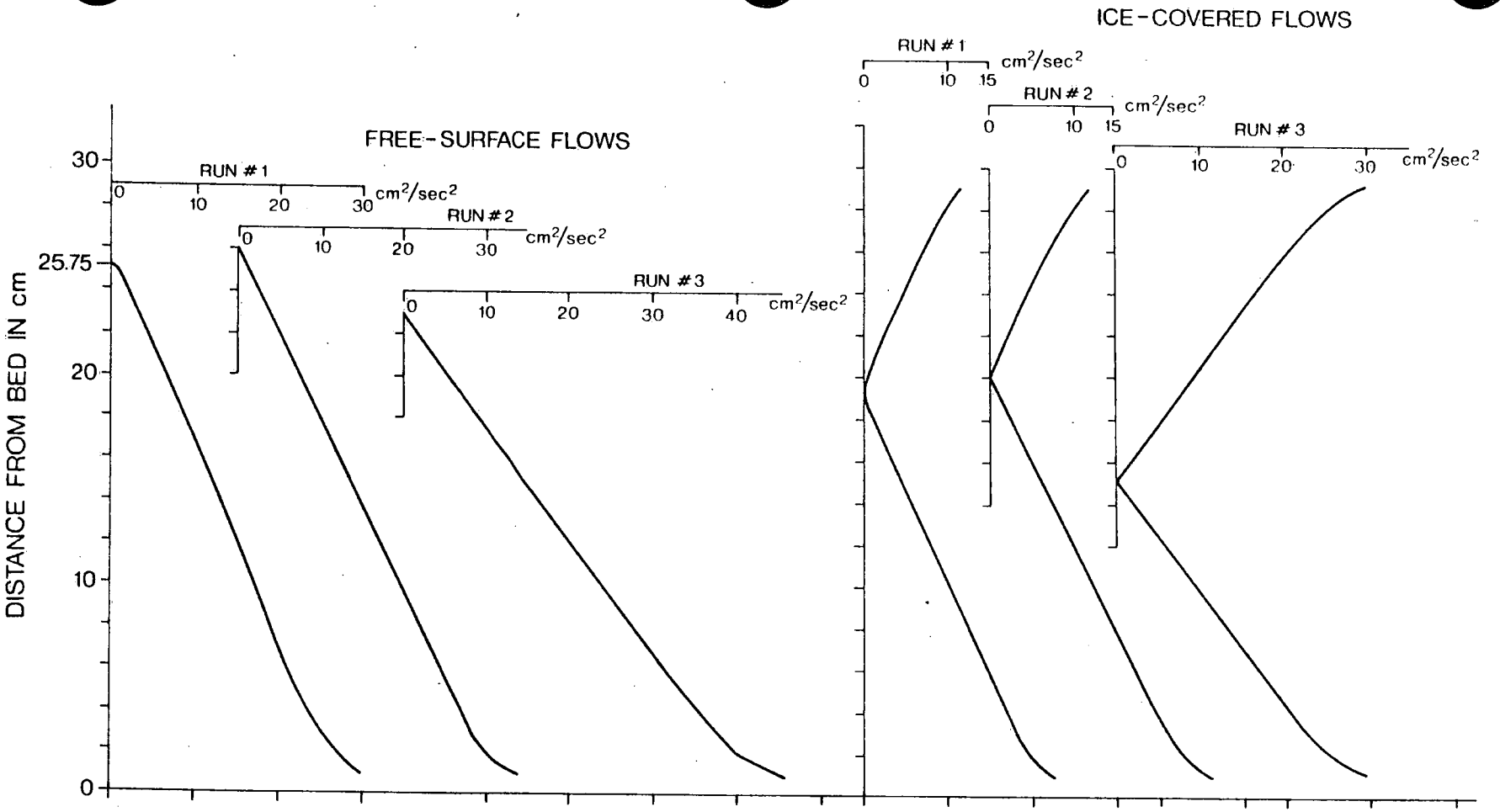

FIGURE 9. SHEAR-STRESS (τ/ρ) DISTRIBUTIONS

tracer as functions of distance from the injection point by solving Eq. 7 with $\sigma_\phi = 1$. The introduction of the tracer was made in the fully developed region of the flows: i.e. at $x > X_o$ and X_i. The sources were of finite width (5 cm) and of uniform concentrations. Three different vertical positions for injections were considered. They were: 1) surface injection, 2) middle injection and 3) bottom injection. The injections were either neutral, where the velocity of the tracer was the same as the ambient flow velocities at the location of the injection, or jet type where the velocity of the tracer was twice that of the ambient flow velocity. Neutral injections were considered for all three runs whereas the jet-type injection was considered only for run no. 1.

Figs. 10, 11 and 12 depict the concentration distributions resulting from three different source positions for run no. 1 for neutral injection. The distributions for run no. 2 and run no. 3 are not shown in this paper to conserve space and because those results were similar to the ones shown in Figs. 10 to 12. In these figures the concentration values are normalized with respect to the concentration at the injection point. The depth axis is not normalized and the actual values are plotted to emphasize the fact that the equivalent depths are different for ice-covered flows and free-surface flows. The centre line of the middle injection was at a depth of 11 cms in both types of flows.

It can be seen from these figures that the reduction in the maximum concentration values is more rapid in the free-surface flows than in the ice-covered flows, indicating that the presence of an ice cover tends to reduce the mixing rate. The difference in the mixing rate is the largest when the injection was at the surface. As the position of injection was moved downwards towards the channel bed, the difference in the mixing rate diminishes.

Figs. 13 and 14 show the velocity and concentration distributions for the jet-type injection. Only the middle injection was considered. As can be seen in

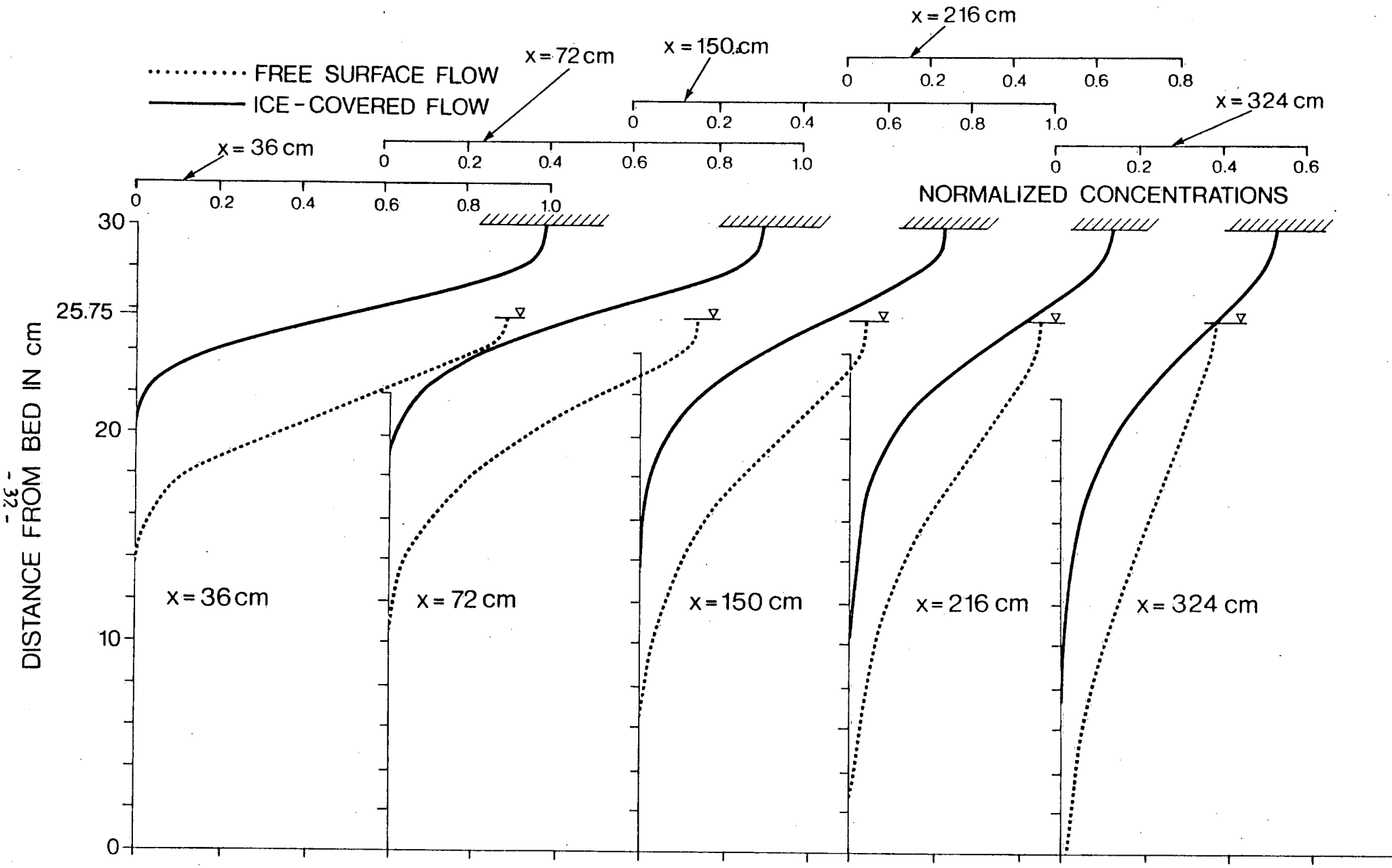

FIGURE 10. CONCENTRATION DISTRIBUTIONS FOR RUN #1 (Surface injection)

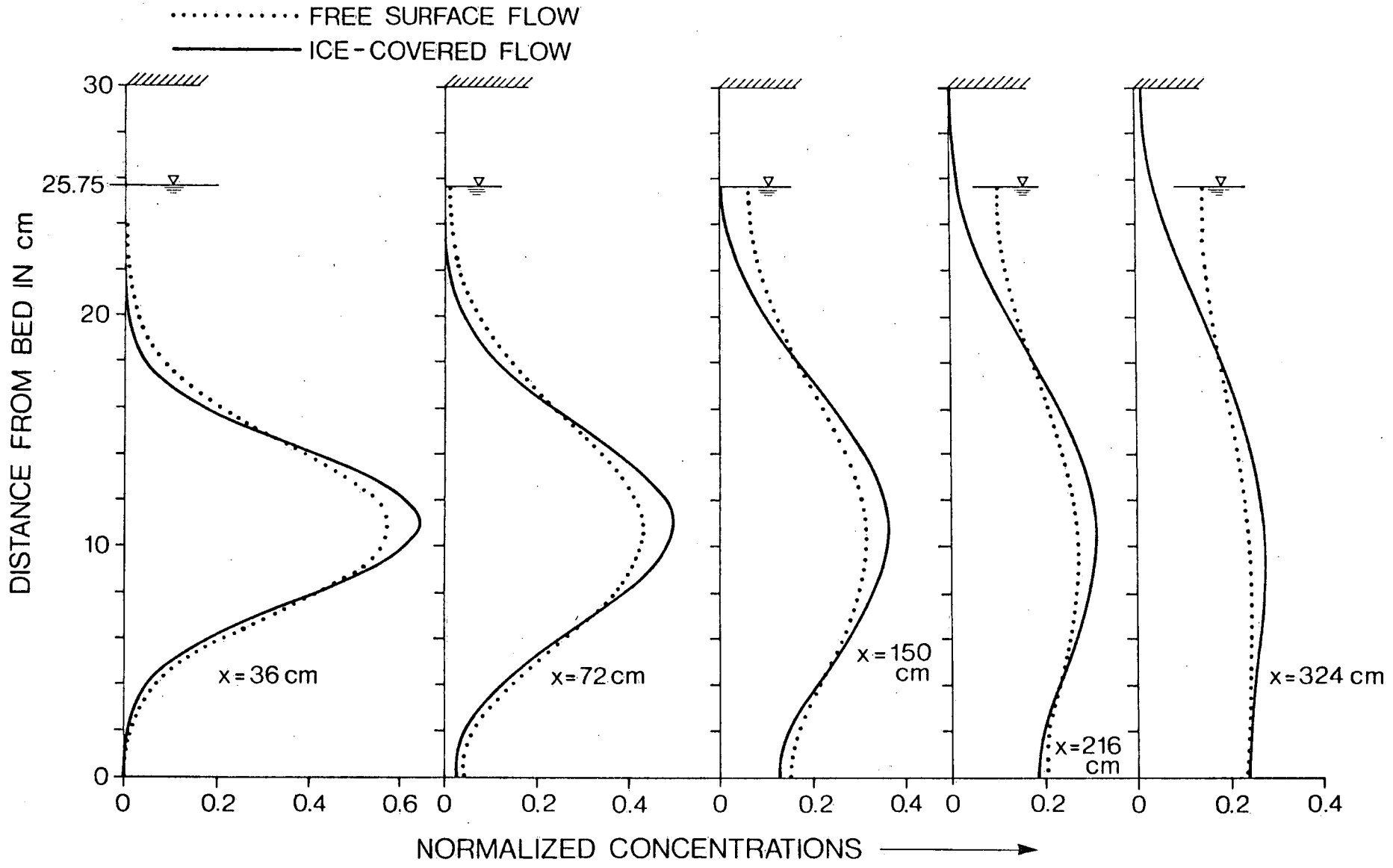

FIGURE 11. CONCENTRATION DISTRIBUTIONS FOR RUN #1 (Middle injection)

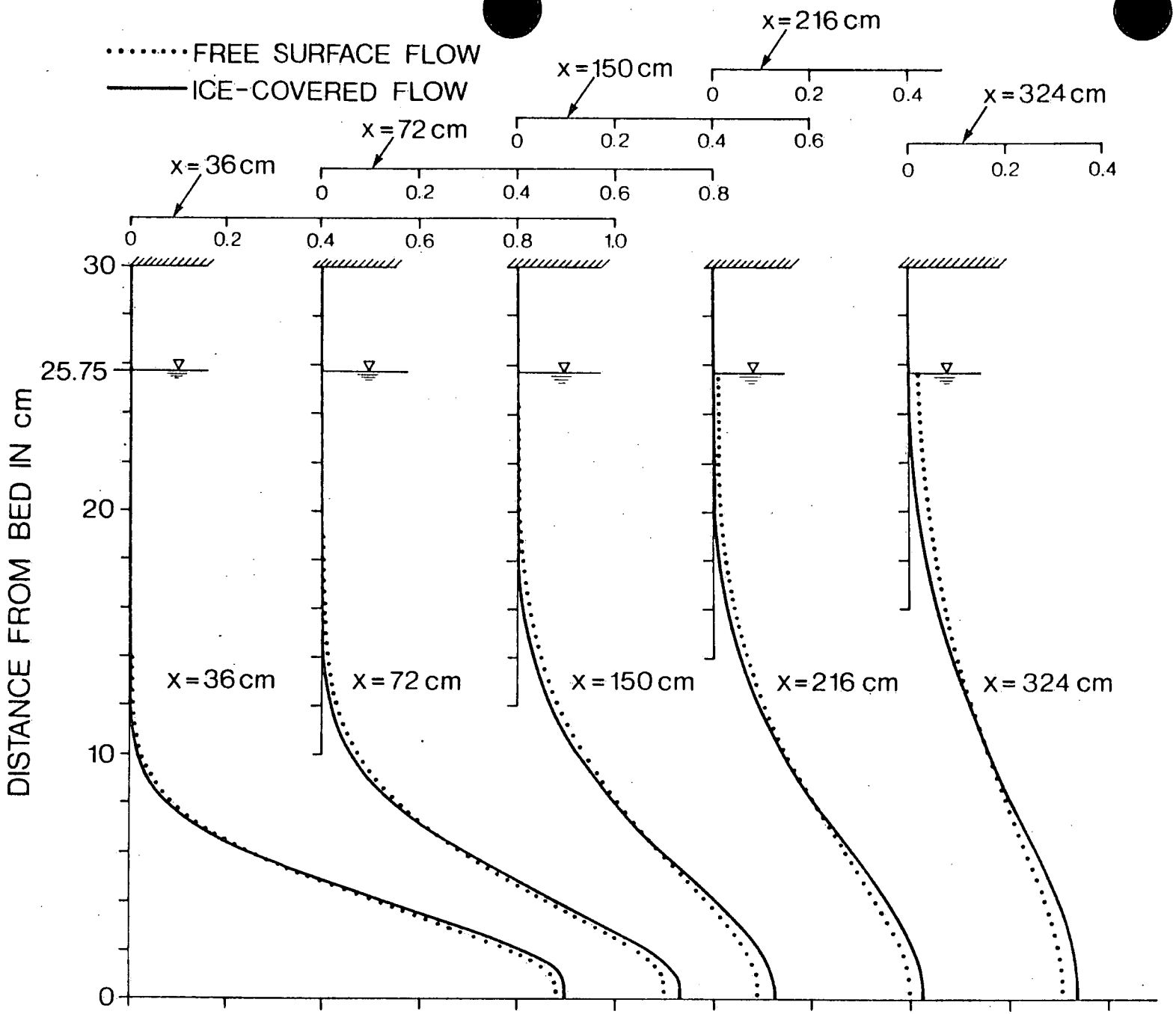

FIGURE 12. CONCENTRATION DISTRIBUTION FOR RUN #1 (Bottom injection)

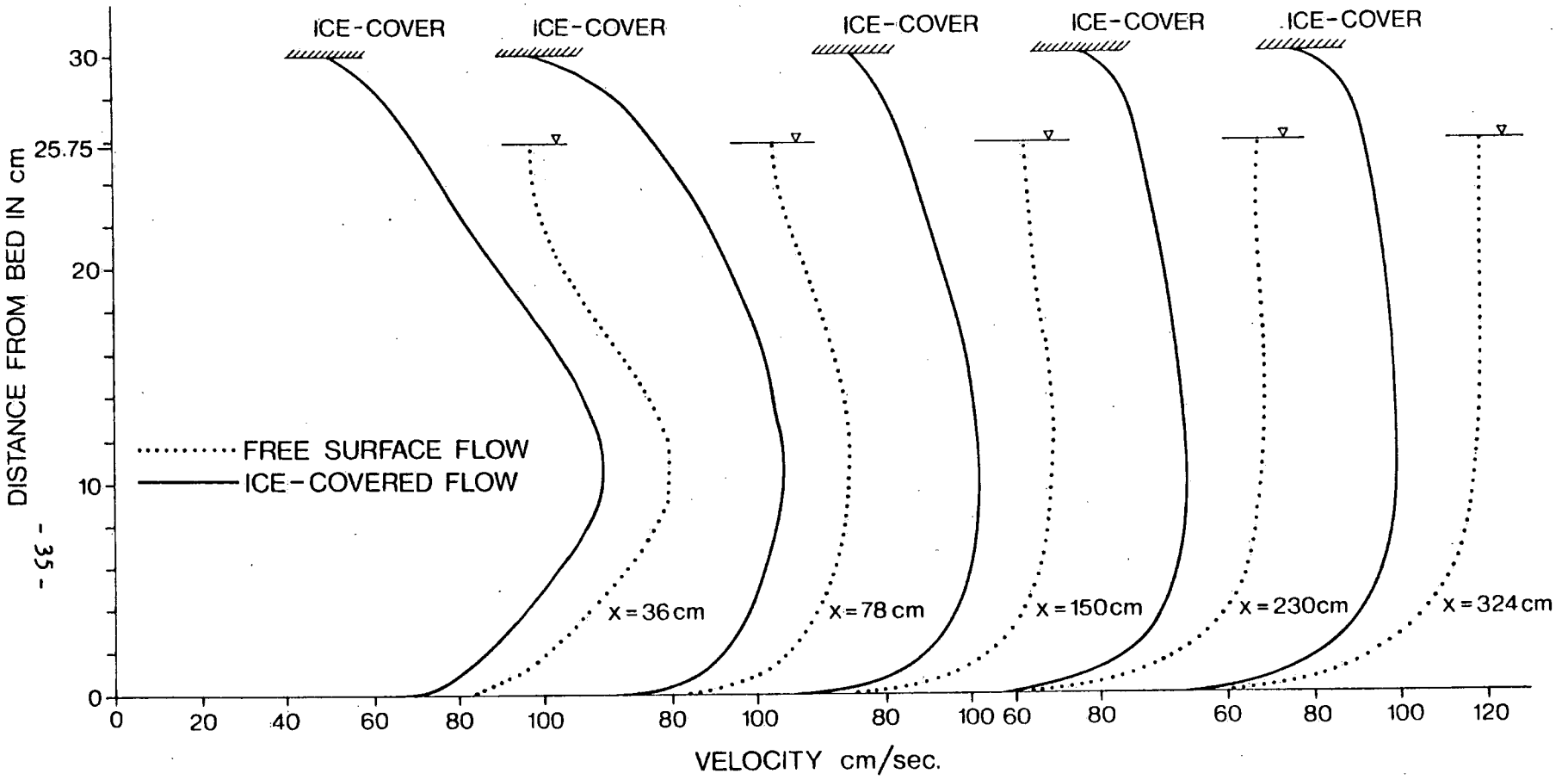

FIGURE 13. VELOCITY DISTRIBUTIONS FOR JET TYPE TRACER INJECTION

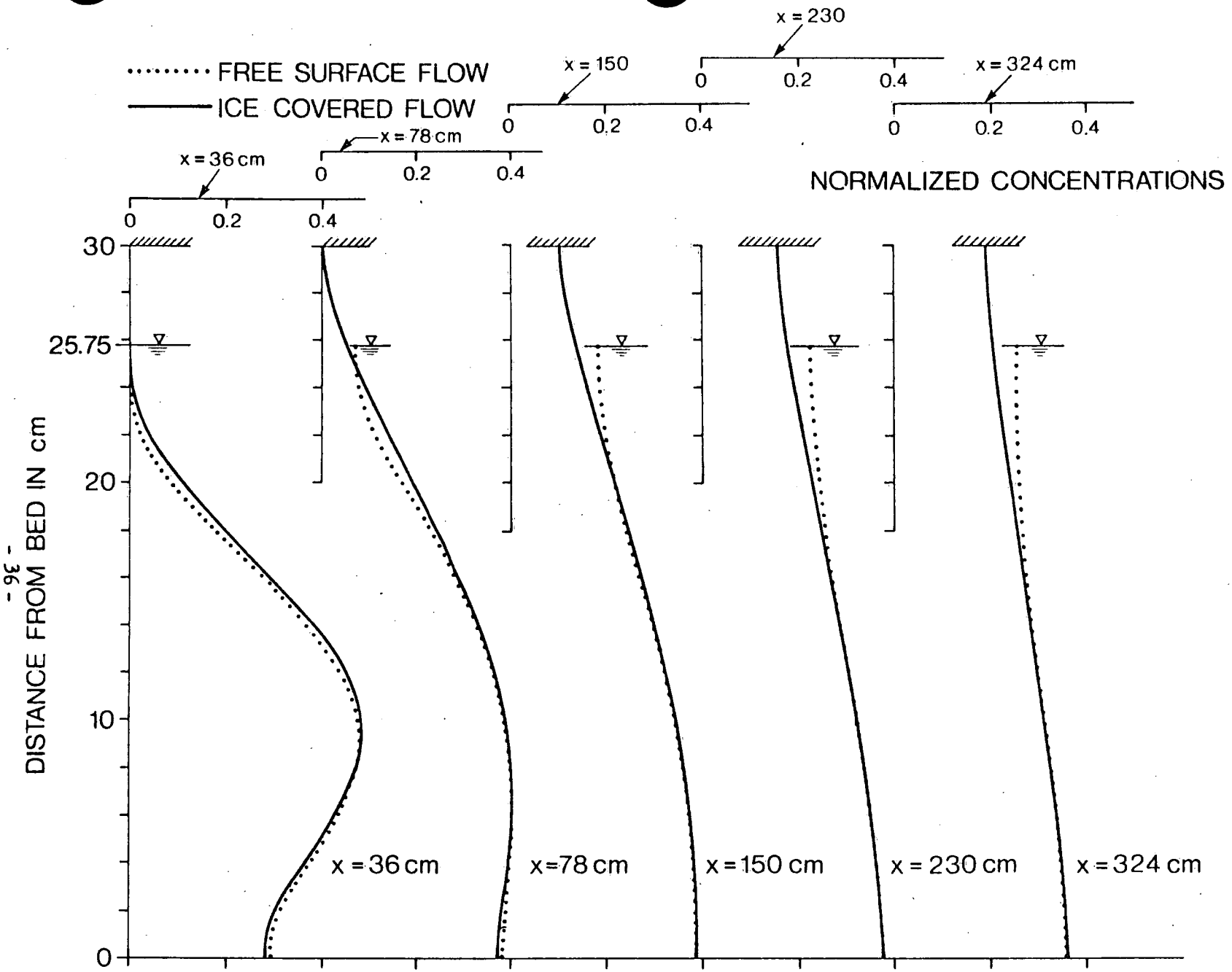

FIGURE 14. CONCENTRATION DISTRIBUTION FOR JET TYPE TRACER INJECTION

Fig. 13, the velocity distribution changes along the length of the channel from the injection location and it becomes invariant with x at about 300 cms from the injection point. The concentration distributions shown in Fig. 14 indicate that the mixing is much faster in the jet-type discharge than in the neutral discharge and the difference between the mixing rates between the open-water flow and the ice-covered flow was not significant for this case.

SUMMARY AND CONCLUSIONS

In this paper, a procedure has been outlined to calculate the fully developed two-dimensional flows in channels with and without ice covers using the k-ε turbulence model proposed by Launder and Spalding (5) and a numerical scheme proposed by Patankar and Spalding (6). Three different fully developed flows were calculated using the procedure for open-water and ice-covered flows. In each case, the flow rate, the channel slope and the roughness of the channel bottom were made to be the same for both open-water flow and ice-covered flow, thereby producing a pair of "equivalent flows". The channel-bed roughness and the ice-cover roughness values were changed from run to run.

The computed velocity and diffusivity distributions do not follow the conventional logarithmic and parabolic distributions for the whole depth of flow. The u distribution deviates slightly from the logarithmic profile for the top 25 percent of the flow, while the ν_t distribution deviates from the parabolic distribution through the top half of the flow. These results tend to agree with the results from recent investigations of velocity distribution (15) and measurements of the diffusivity distribution (2), thus giving confidence to the calculations from the k-ε model.

In all cases, the equivalent ice-covered flows have larger flow depths and smaller bed shears than the free-surface flows. The resulting diffusivities are smaller than the free-surface flow values. However, the diffusivity does not go to zero and the arbitrary modification of the diffusivity profile which other flow models employ is not required in this model.

Concentration distributions resulting from the introduction of a neutrally buoyant tracer were computed for all the runs and these distributions indicate reduced mixing rates in ice-covered flows compared to the open-water flows. The difference in mixing rates was larger when the location of injection of the tracer was closer to the upper boundary. However, the results from using a jet-type injection gave approximately the same concentrations for the ice-covered and free-surface flows, which indicate that the effects of jet mixing outweigh the difference in the diffusivity.

APPENDIX I. - REFERENCES

1. Ismail, H. M., "Turbulent Transfer Mechanism and Suspended Sediment in Closed Channels," Transactions, ASCE, Vol. 11, 1952, pp. 409-446.
2. Jobson, H. E., "Vertical Mass Transfer in Open Channel Flow," Thesis presented to Colorado State University at Fort Collins, Colorado in 1968 in partial fulfillment of the requirement for the degree of Doctor of Philosophy.
3. Larsen, P. A., "Head Losses Caused by an Ice Cover on Open Channels," Journal of the Boston Society of Civil Engineers, Vol. 45, No. 1, 1968, pp. 45-67.
4. Larsen, P. A., "Hydraulic Roughness of Ice Covers," Journal of the Hydraulics Division, ASCE, Vol. 99, No. HY1, 1973.
5. Launder, B. E., and Spalding, D. B., "The Numerical Calculation of Turbulent Flows", Computer Methods in Applied Mechanics and Engineering, Vol. 3, 1974, pp. 269-289.
6. Patankar, S. V. and Spalding, D. B., "Heat and Mass Transfer in Boundary Layers," Intertext publishers, London, England, 1970.
7. Rastogi, A. K., and Rodi, W., "Predictions of Heat and Mass Transfer in Open Channels," Journal of the Hydraulics Division, ASCE, Vol. 104, No. HY3, 1978.
8. Sayre, W. W., "Dispersion of Mass in Open Channel Flow," Hydrology Paper No. 75, Colorado State University, Fort Collins, Colorado, 1975.
9. Sayre, W. W., and Song, G. B., "Effects of Ice Covers on Alluvial Channel Flow and Sediment Transport Processes," IIHR Report No. 218, Iowa Institute of Hydraulic Research, University of Iowa, Iowa, 1979.

10. Shen, H. T., and Harden, T. O., "The Effects of Ice Cover on Vertical Transfer in Stream Channels," Water Resources Bulletin, American Water Resources Association, Vol. 14, No. 6, 1978.

11. Song, C.C.S., and Yang, C. T., "Velocity Profiles and Minimum Stream Power," Journal of the Hydraulics Division, Proc. ASCE, Vol. 105, No. HY8, 1979.

12. Uzuner, M. S., "The Composite Roughness of Ice-Covered Streams," Journal of Hydraulics Research, IAHR, Vol. 13, No. 1, 1975, pp. 79-102.

13. Vanoni, V. A., "Transportation of Suspended Sediment by Water," Transactions, ASCE, Vol. 111, Paper 2267, 1946, pp. 67-102.

APPENDIX II - NOTATION

The following symbols are used in this paper:

c_1, c_2, c_μ = empirical constants;

E = roughness parameter;

g = acceleration due to gravity;

G = rate of production of turbulent energy;

h = flow depth;

i = subscript denoting ice-covered flow;

I = grid location in the longitudinal direction;

J = grid location in the vertical direction;

K_s = equivalent sand grain roughness;

k = kinetic energy of turbulent motion;

o = subscript denoting free surface flow;

q = per unit width;

S = slope of channel bed;

s = source term;

u = velocity component in the longitudinal direction;

v = velocity component in the vertical direction;

v_* = shear velocity;

w = subscript denoting values close to wall regions;

X = longitudinal distance where the flow attains fully developed state;

$\grave{x}$ = cartesian co-ordinate in the longitudinal direction;

y = cartesian co-ordinate in the vertical direction;

Γ_y = mass transfer coefficient in the y direction;

Δx = distance between grid points in the x direction;

Δy = distance between grid points in the y direction;

ε = rate of dissipation of turbulent energy;

κ = Von-Karmon constant;

ν_t = turbulent eddy viscosity;

ν = kinematic viscosity of fluid;

ρ = fluid density;

$\sigma_t, \sigma_\varepsilon, \sigma_\phi$ = empirical constants;

τ = shear stress;

ϕ = scalar quantity.

CIVIL ENGINEERING ABSTRACT: The flow and mixing characteristics of free-surface and ice-covered flows were computed using the k-ϵ turbulence model. The results deviate from the conventional distributions; but are in general agreement with measurements reported in the literature.

158

ENVIRONMENT CANADA LIBRARY, BURLINGTON
3 9055 1016 7605 3